Subwavelength optical imaging of evanescent fields using reflections from plasmonic slabs

Matthew D. Arnold[1,2*] and Richard J. Blaikie[1]

[1]*MacDiarmid Institute for Advanced Materials and Nanotechnology and Department of Electrical and Computer Engineering, University of Canterbury, Private Bag 4800, Christchurch, New Zealand*

[2]*Current address: Physics and Advanced Materials, University of Technology Sydney, PO Box 123, Broadway NSW 2007, Australia*

[*]*Corresponding author: Matthew.Arnold-1@uts.edu.au*

Abstract: Reflection can significantly improve the quality of sub-wavelength near-field images, which is explained by appropriate interference between forward and reflected waves. Plasmonic slabs may form approximate super-mirrors. This paper develops general theory in both spectral and spatial representations that allows the reflector position and permittivity to be determined for optimum image uniformity. This elucidates previous observations and predicts behaviour for some other interesting regimes, including interferometric lithography.

OCIS codes: (100.6640) Super-resolution; (110.5220) Photolithography; (260.3910) Metals, optics of; (240.6680) Surface plasmons.

References and links

1. J. B. Pendry, "Negative refraction makes a perfect lens," Phys. Rev. Lett. **85**, 3966-3969 (2000).
2. J. S. Wei and F. X. Gan, "Dynamic readout of subdiffraction-limited pit arrays with a silver superlens," Appl. Phys. Lett. **87**, art. no. 211101 (2005).
3. T. Taubner, D. Korobkin, Y. Urzhumov, G. Shvets, R. Hillenbrand, "Near-field microscopy through a SiC superlens," Science **313**, 1595-1595 (2006).
4. D. O. S. Melville and R. J. Blaikie, "Super-resolution imaging through a planar silver layer," Opt. Express **13**, 2127-2134 (2005)
5. N. Fang, H. Lee, C. Sun, X. Zhang, "Sub-diffraction-limited optical imaging with a silver superlens," Science **308**, 534-537 (2005).
6. R. J. Blaikie, M. M. Alkaisi, S. J. McNab, D. O. S. Melville, "Nanoscale optical patterning using evanescent fields and surface plasmons," Int. J. Nanoscience **3**, 405-417 (2004)
7. D. B. Shao and S. C. Chen, "Surface-plasmon-assisted nanoscale photolithography by polarized light," Appl. Phys. Lett. **86**, art. no. 253107 (2005)
8. D. B. Shao and S. C. Chen, "Numerical simulation of surface-plasmon-assisted nanolithography," Opt. Express **13**, 6964-6973 (2005).
9. M. D. Arnold and R. J. Blaikie, "Using surface-plasmon effects to improve process latitude in near-field optical lithography," in Proceedings of the International Conference on Nanoscience and Nanotechnology, Brisbane, Australia, IEEE Press 06EX1411C, 548-551 (2006).
10. M. Schrader, M. Kozubek, S. W. Hell, T. Wilson, "Optical transfer functions of 4Pi confocal microscopes: theory and experiment," Opt. Lett. **22**, 436-438 (1997).
11. B. W. Smith, Y. Fan, J. Zhou, N. Lafferty, A. Estroff, "Evanescent wave imaging in optical lithography," Proc. SPIE **6154** (2006)

1. Introduction

Near-field imaging transfers sub-wavelength information via evanescent waves, however the exponential decay of these waves usually means that image quality decays rapidly with distance from the object. It can be shown that a slab of material supporting coupled surface states such as polaritons makes a useful near-field super-lens [1], as demonstrated in important techniques such as data-storage [2], microscopy [3] and lithography [4,5].

#84156 - $15.00 USD Received 14 Jun 2007; revised 20 Aug 2007; accepted 21 Aug 2007; published 27 Aug 2007

However, such lenses are significantly aberrated by loss and dispersion, and alternative techniques to manipulate near-field images would be clearly advantageous.

Mirrors are a classical replacement for lossy lenses, and it has been proposed [6] that metal slabs can act as super-mirrors in the near-field by regenerating evanescent waves, and that image quality is improved compared to the image without reflection. Some aspects of near-field reflection imaging have been experimentally and theoretically demonstrated [7,8]. Recently we simulated near-field imaging of absorbing objects with single layer reflectors [9] and empirically determined some desirable conditions: TM polarization, reflector permittivity approximately the negative of the imaging layer, and object-reflector distance tuned according to object size. We return to this problem with a more rigorous approach, and present a general theory for attaining improved imaging using reflections.

Conventional wisdom suggests that reflections might produce poor images due to standing wave effects, and in many situations reflections are suppressed by index-matched surfaces [6]. This apparent conflict can be resolved using the methods presented here, which can be applied to new geometries where evanescent fields are important. Essentially, interference of the forward and reflected fields longitudinally symmetrizes the response, leading to improvements such as those listed above. This has some analogies with 4-pi microscopy [10], but the technique presented here only requires one-directional illumination. The theme of this article is that control of quality of the near-field image can be achieved by control of the amplitude and phase of the reflection.

We first sketch the problem that we are trying to solve. The geometry of reflection imaging that has been previously considered [6-9] is shown in Fig. 1. We use this as a starting point for discussion, noting that we wish to develop a general theory that could be applied to other geometries. A planar object is shown aligned parallel to the y-z plane—a periodic binary absorber for the example in Fig. 1—with the object's exit plane located at $x = d$. A reflector of some kind is located at $x = 0$ and the system is illuminated from the right with light of wavelength λ. It is the evolution of the optical fields in the imaging region, $0 < x < d$, that is of interest here, both with and without the reflector. We consider a non-perturbative imaging medium, such as a weakly absorbing photoresist filling the imaging region [4-8], as scanning-probe image detection (e.g. Ref. [3]) could produce significant field perturbations that we do not wish to consider here.

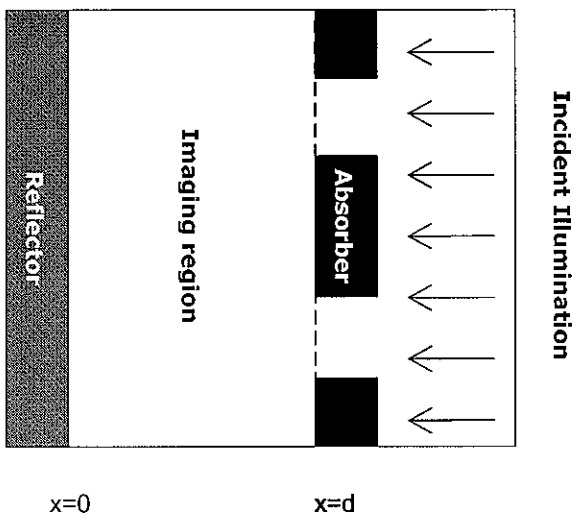

Fig. 1. Imaging situation under consideration here. An object at $x = d$ is illuminated from the right, and the effects of a reflector at $x = 0$ are studied in the imaging region $0<x<d$.

#84156 - $15.00 USD Received 14 Jun 2007; revised 20 Aug 2007; accepted 21 Aug 2007; published 27 Aug 2007

The general problem is how to predict the image quality assuming an arbitrary object (with arbitrary reflector parameters). We first need to discuss how we define an image, referring to examples of near-field imaging with and without reflection as shown in Fig. 2. The object lies at $x = d$, which may also be considered an 'exact' image plane (i.e. it is the fields at this plane that we wish to transfer throughout our imaging volume). The fields evolve right-to-left along the longitudinal axis x, forming an extended near-field image. Any reflected fields (associated with an apparent reflected image) combine with the forward-going fields, and we will call the result 'the image' for brevity. With no-reflection the image is longitudinally asymmetric (Fig. 2(a)), but reflection increases symmetry (Fig. 2(b)) which can improve uniformity. This extended image can be summarized in terms of intensity profiles on medial planes (Fig. 2(c) & (d)) under light (I_1) and dark (I_0) features of the object, which can be used to calculate various image metrics.

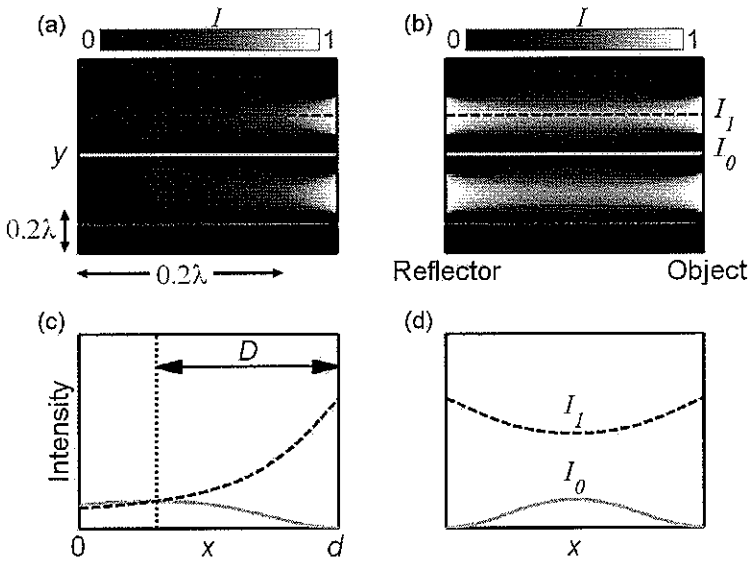

Fig. 2. Image geometry in two-dimensions, the third being invariant. A hypothetical (but representative) image with no reflection is shown in (a) and with reflection (b). The medial longitudinal profiles I_0 and I_1 as marked in (a),(b) are shown in (c),(d). Limited depth-of-field D is indicated in (c).

Referring to Fig. 2, we define local contrast $\gamma(x) \equiv I_1(x)/I_0(x)$ at distance $d-x$ from the object, and global contrast $\Gamma = \min(I_1)/\max(I_0)$ over the whole imaging domain $0 \le x \le d$. An alternative measure of contrast is visibility $V = (\Gamma - 1)/(\Gamma + 1)$, and the depth-of-field D is given by the distance over which $V > 0$, as shown in Fig. 2(c). Imaging applications such as lithography usually have minimum requirements for both global contrast and depth-of-field, but evanescent decay results in competition between these two important metrics. In this paper we use reflection to improve the tradeoff between global contrast and depth-of-field.

2. Theory of reflection imaging

We now develop a theory for reflection imaging, the premise being that if we know the object field we can predict the extended image. In this exposition we aim for brevity by starting with a single field component H, which allows us to show some generic aspects of field evolution including reflection. We make a number of assumptions including 2D spatial dependence of the three-component fields with in-plane propagation and isotropic homogeneous media.

#84156 - $15.00 USD Received 14 Jun 2007; revised 20 Aug 2007; accepted 21 Aug 2007; published 27 Aug 2007

These assumptions allow us to show important behavior with simpler theory and do not necessarily limit the results to those shown here.

Referring to Fig. 2, we aim to predict the spatial dependence of the field $H(x,y)$ in the imaging region bounded by $0 \le x \le d$, assuming knowledge of the object field $H(d,y)$. The field can be rewritten as a superposition of sinusoidal plane-waves (implicitly $\exp(-i\omega t)$), which may be reflected at $x = 0$ due to differences in the wave-number k in different media. The lateral propagation constant β is conserved, and longitudinal propagation is $\alpha = \sqrt{k^2 - \beta^2}$ where the imaginary part should be non-negative to ensure causality. When $\beta > k$ then α is purely imaginary corresponding to evanescent components. The spectral components are represented by complex wave amplitudes, strictly written $h(x,\beta)$, but henceforth we shall omit β for spectral functions.

A cavity formed by the mirror at $x = 0$ and the interface at the object could result in multiple reflections, but it is most convenient to consider the aggregate forward and reflected fields related by the reflectance r of the mirror. The spectral representation for the aggregate forward object (at the object plane) is written $h^f(d)$, and the reflection (also referenced to the object plane) is $h^r(d) = re^{i\alpha 2d} h^f(d)$. To get the total spatial field $H(x,y)$ throughout the imaging region we can add forward and reflected fields, accounting for $e^{\pm i\alpha x}$ propagation in the x direction:

$$H(x,y) = \int_{\beta=-\infty}^{\infty} \left[e^{i\alpha(-x+d)} + re^{i\alpha(x+d)}\right]\left[h^f(d)\right]e^{i\beta y} d\beta = G_H^f(d,x,y) * H^f(d,y). \quad (1)$$

The integral in Eq. (1) is a Fourier transform mapping $\beta \leftrightarrow y$, and $*$ denotes spatial convolution of the forward object $H^f(d,y)$ with a line-spread function (LSF) G_H that is a property of the imaging system (separation d and mirror reflectivity r). The Fourier transform of this LSF is an optical transfer function (OTF) g_H^f, which we can use to write Eq. 1 in the spectral domain such that $h^f(x) = g_H^f h^f(d)$.

In some cases it may be more convenient to work with the total object $h(d) = h^f(d) + h^r(d)$. Explicitly we wish to find an OTF g_H such that $h(x) = g_H h(d)$, and it is not hard to show that $g_H = g_H^f / g_H^f(x = d)$ where the denominator is evaluated at $x=d$. Rewriting in real-space, we can use $H(x,y) = G_H * H(d,y)$ to determine the total field throughout the imaging region in terms of the total field at the object ($H(d,y)$) and the new LSF (G_H).

The reflectivity r is complex-valued quantity which, for convenience, can be mapped as a translation by a "distance" $-2X$ such that $r = \pm e^{-i\alpha 2X}$, and thus the OTF is rewritten

$$g_H^f = e^{i\alpha(d-X)}\left[e^{i\alpha(-x+X)} \pm e^{i\alpha(x-X)}\right]. \quad (2)$$

If X is constant and real, two special planes can be identified from the OTF. For a positive reflection $x = X$ is a symmetry plane, and $x = -d + 2X$ is the corresponding exact image plane due to reflection. Logically, for negative reflections we have anti-symmetry and an anti-image. The reflected image may actually lie outside the imaging region itself, but this virtual image still affects the fields inside the imaging region. If X is not real but α is either purely real or imaginary, it can be shown that Re(X) is a conjugate symmetry plane where the magnitude is symmetric but the phase relationship of the images is complicated. Note carefully that the reflected image is exact so long as the conditions above are met, particularly the requirement for constant X.

The inverse mapping back to X from the reflectance r and propagation constant α is

$$X = \frac{\ln|r| + i\left[\arg(\pm r) + m2\pi\right]}{-2i\alpha}, \quad (3)$$

#84156 - $15.00 USD Received 14 Jun 2007; revised 20 Aug 2007; accepted 21 Aug 2007; published 27 Aug 2007

which describes the symmetry plane due to reflection. This mapping is complex and may be multi-valued, which gives rise to rich behaviour. Propagating components (α real) have multiple values of Re(X), meaning there are multiple images interspersed with anti-images, resulting in the usual longitudinal standing waves which are generally undesirable. Evanescent components (α imaginary) have only one value, which simplifies control of imaging.

As we shall see, image uniformity is optimized when the symmetry plane lies in the middle of the imaging space ($X = d/2$), placing the exact reflected image of the object plane fields on the reflector surface ($x = 0$). However, note that the reflection mapping has an explicit dependence on α (and hence on β) which means that X generally varies with spatial frequency. Hence it may not be possible to achieve exact images, but a possible strategy is to choose a symmetry plane based on the dominant spatial frequencies in the object. Alternatively, the special case $r = \pm 1$ sets the symmetry plane at the reflector surface ($X = 0$) regardless of α.

2.1 Plasmonic reflectors

We can now consider a possible way to achieve the desired reflection, which may require enhancement of the evanescent fields by using plasmonic reflectors. Let us assume non-magnetic materials, with the imaging region ($0 < x < d$) having permittivity ε and a semi-infinite mirror with permittivity ε_r, so the relationship between media (k) and vacuum (k_0) wave-numbers is $k^2 = \varepsilon k_0^2$. In this case only TM polarization allows evanescent amplification, in which case the magnetic field is H as given by Eq. (1) above. Actually, we are primarily interested in electric fields, and the x and y components of the electric field can be similarly calculated by their respective OTFs:

$$\begin{aligned} g_{Ey}^f &= -e^{i\alpha(-x+d)} + re^{i\alpha(x+d)} \\ g_{Ex}^f &= -e^{i\alpha(-x+d)} - re^{i\alpha(x+d)} \end{aligned}. \tag{4}$$

where the spectral electric objects are $e_y(d) = h(d)\alpha/\omega\varepsilon$ and $e_x(d) = h(d)\beta/\omega\varepsilon$. Note that the spatial field E_x has the same type of symmetry as H, but E_y is the opposite. Then the reflectivity is

$$r = \frac{\varepsilon_r \alpha - \varepsilon \alpha_r}{\varepsilon_r \alpha + \varepsilon \alpha_r}. \tag{5}$$

where the r subscript indicates the reflector medium, and lack of a subscript indicates the imaging medium.

Proper physical constraints dictate a finite thickness reflector, but it can be shown that even moderately thin layers approach the asymptotic limit if permittivity is lossy or negative. Equation (5) can be rearranged to give the required reflector permittivity:

$$\frac{\varepsilon_r}{\varepsilon} = \frac{1 \pm \sqrt{1 - 4(\beta/k)^2 f^2}}{2f^2}, \tag{6}$$

where

$$f = \frac{\alpha(1-r)}{k(1+r)} = \frac{2\alpha \tan(\alpha X)}{ik}. \tag{7}$$

Note that the square root in Eq. (6) implies two possible solutions for permittivity but only one is correct, which should be determined by back-substitution into (5). Equation (7) gives both a general solution (in terms of arbitrary reflectance r) and an imaging-specific solution (in terms of symmetry plane X).

#84156 - $15.00 USD Received 14 Jun 2007; revised 20 Aug 2007; accepted 21 Aug 2007; published 27 Aug 2007

Low spatial dispersion of the symmetry plane is required for good images, and examples of the spatial-frequency dependence of the optimized reflector permittivity ε_r and object-mirror separation d are shown in Fig. 3. Analysis of Eq. (6) shows that the permittivity for the negative solution is usually smooth and relatively flat across a range of β whereas the positive solution is not, so unless otherwise stated, only the negative solutions are plotted in Fig. 3. Referring to Fig. 3(a), the far evanescent limit ($\beta \to \infty$) is given by $\varepsilon_r \to -\varepsilon$ which is independent of d and is the same condition as required for plasmonic super-lensing [1]. Another useful limit is $\lim_{\beta \to 0} \varepsilon_r = -\varepsilon \tan^2(kX)$, which determines the response for the low-spatial frequency (dc) image components; if this is matched to the far-evanescent limit we find a reasonable choice for the symmetry plane at $X = \pi/(4k)$, which implies quarter-wavelength for d. We can also consider the dispersion of the image plane under fixed permittivity, shown in Fig. 3(b). It can be shown that there is a pole corresponding to the surface plasmon, $\beta = k_0\sqrt{\varepsilon\varepsilon_r/(\varepsilon+\varepsilon_r)}$, where the imaging behaviour is unstable and so this region should be avoided.

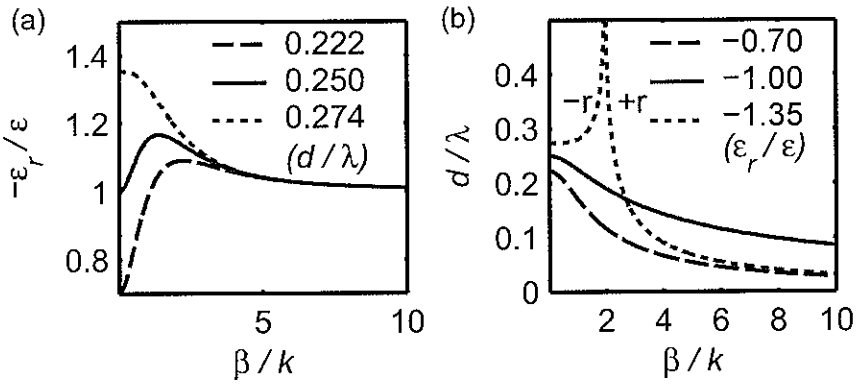

Fig. 3. Movement of optimized parameters as a function of β: (a) optimized reflector permittivity for various object-mirror separations d and (b) optimized object-mirror separations for various permittivities. All reflections "negative" except as noted.

It may be possible to achieve even flatter spatial dispersion than is shown in Fig. 3 by using multiple layers, anisotropy or meta-materials for the reflector, but we leave that task for the future. However, we note that choosing a symmetry plane at the substrate allows two dispersionless solutions. The positive solution requires $|\varepsilon_r| \to \infty$ which could be provided by metals, absorbers or high-index dielectrics, and the negative solution requires $|\varepsilon_r| \to 0$ corresponding to metals at the plasma frequency.

3. Representative results

We now examine the detailed behavior of the LSF for some reflectors, since this describes the evolution of images. Whilst it is easiest to calculate the LSF numerically using fast Fourier transforms (FFT), accuracy for perfect reflectors can be compared to an analytic solution in terms of the forward object:

#84156 - $15.00 USD Received 14 Jun 2007; revised 20 Aug 2007; accepted 21 Aug 2007; published 27 Aug 2007

$$G^I = i\pi \sum_{j=1}^{2} \left[H_1^{(1)}\left(\sqrt{x_j^2 + y^2}\right) x_j \Big/ \sqrt{x_j^2 + y^2} \right]$$
$$x_1 = -x + d \qquad (8)$$
$$x_2 = +x + d - 2X$$

where $H^{(1)}$ is the Hankel function of the first kind. This LSF corresponds to the sum of cylindrical contributions from the object and the mirror image. Unfortunately there is no simple expression for total objects or general interfacial reflections, and so we now look at numerical results generated via FFT of Eq. (4). In general the LSF should primarily be laterally narrow and secondarily be longitudinally uniform.

The relative "width" of the LSF is shown in Fig. 4 for various imaging scenarios. Specifically, for each d we calculated a LSF in (x,y) space, drew a contour level with the longitudinal minimum along the central ridge, and took the maximum width of the region enclosed by the contour. First, comparing the free-space case ($r = 0$) to the other cases, the overall width can be made to decrease significantly for a range of d by the use of a reflector, highlighting the main point of this paper that reflections can improve image quality. But note that the width can also become much greater than for the no-reflection case if the imaging geometry is not chosen correctly. The no-reflection case (dashed) scales as width/d~1, whereas with reflection (dotted) scaling goes like width/$(d-X) \sim 1$, at least up to $d-X \sim \lambda/4$ where standing wave effects begin to make reflection undesirable. As expected, maximum performance is attained when the exact reflected image lies on the reflector surface ($X = d/2$), although there is some improvement when the symmetry plane lies on the reflector surface ($X = 0$). Now considering the $\varepsilon_r = -\varepsilon$ case, the concept of an exact image is broken due to the dispersion of the symmetry plane. There is a virtual singularity at $x = -d$ which has some characteristics of an image, but it is severely distorted so symmetry considerations are most useful for characterizing the depth of the extended image. The symmetry plane dispersion runs across $0 \le X \le \lambda/8$, so thicknesses in the range $\lambda/8 \le d \le \lambda/4$ are expected to be ideal. Indeed, when compared to no reflection there is significant improvement in uniformity and width, and performance often approaches that of the perfect case.

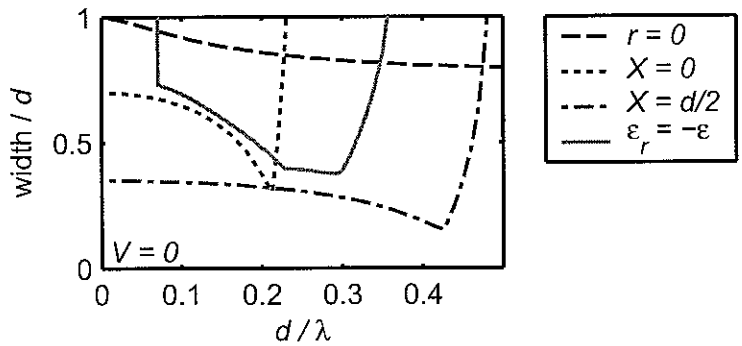

Fig. 4. Comparison of scaled widths (width/d) for the LSF G_{Ey} versus image thickness d for various reflectors. Widths are maximums over the imaging region, corresponding to LSF contours at intensity $I_0 = \min(I_1)$.

Note that in this section only results for the total-to-total LSF for E_y have been shown. In general all types of transfer functions exhibit similar behavior (i.e. reflection narrowing) in some regime, but this is highly dependent on the symmetry of reflection for that component and in general each component should be considered separately. The choice of the particular type of transfer function depends on the nature of the physical object, but there is good

#84156 - $15.00 USD Received 14 Jun 2007; revised 20 Aug 2007; accepted 21 Aug 2007; published 27 Aug 2007

justification of using total-to-total transfers. These can be directly applied to information provided by many simulations and we shall see soon that this is most appropriate for some common types of object.

Also note that we have made the usual assumption of a non-absorbing imaging medium. Actually a certain amount of absorption is required for the imaging medium in lithography, but the absorption is typically designed to compromise between sufficient sensitivity and low perturbation for far-field exposures. Near-field exposures require more careful consideration of wave propagation, but it turns out that only spatial frequencies with $\beta/k \sim 1$ are significantly damped and far-evanescent frequencies are actually least affected. Hence sub-diffraction-limited exposures are not likely to be significantly degraded.

That concludes a general discussion of the imaging behaviour, and we now turn our attention to details relating to specific objects. Whilst the LSF describes important behaviour, the object field actually depends on the reflection so generally numerical techniques are required to determine a full solution. Fortunately many types of objects are amenable to simple modeling, and we choose two such objects as examples, one old and one new.

3.1 Binary absorber objects

One system previously considered has been imaging of binary absorber objects [6-9], such as the binary absorber shown in Fig. 5. In this case we assume that the TM source wave is normally incident on scatterers which have features with some degree of lateral symmetry. The result is lateral symmetry in tangential fields throughout the imaging region and anti-symmetry in the scattered normal field. Hence feature symmetry planes have vanishing normal electric field leaving the tangential electric field dominant. We will ignore the magnetic field because electric fields usually dominate appropriate light matter interactions. TM polarization has tangential object fields with two basic contributors: geometric transmission and edge diffraction which produces large spikes at sharp feature edges, as seen in Fig. 5(b). Hence basic behavior can be described using only the tangential electric LSF, and so much of the observed improvements are described by the earlier discussion.

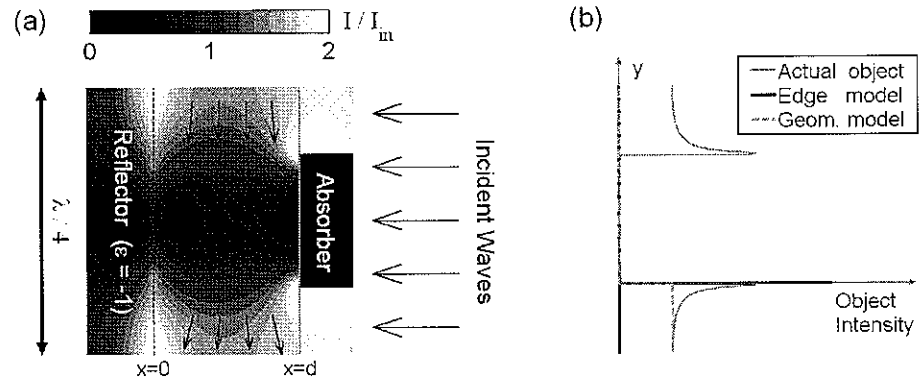

Fig. 5. An example of an image of a binary absorber of width a using a plasmonic reflector. The full image is shown in (a), with field line direction confirming dominant tangential fields. A cross-section of the object field at the exit of the absorber (green line) is shown in (b), with model contributions overlaid (edge diffraction blue and geometric transmission cyan).

Further, the dark region (directly beneath the center of the absorber) is most critical for contrast because blurring transfers energy from light-to-dark, and not vice-versa. Noting that the dark region is due to absorbers which produce minimal total fields, there is clear justification for concentrating on the total-to-total LSF along the dark plane. Further, side-lobes in the LSF for $\varepsilon_r = -\varepsilon$ have a critical effect on the dark plane, and we now show that

#84156 - $15.00 USD Received 14 Jun 2007; revised 20 Aug 2007; accepted 21 Aug 2007; published 27 Aug 2007

this explains the strong correlation between absorber width a and optimum d that was previously observed [9].

We have modeled optimum contrast d - a curves (Fig. 6) by approximating the longitudinal evolution of the image along the medial dark-plane. Image evolution was estimated by convolving the total-to-total LSF for E_y with an idealized total object field that is assumed to be independent of reflection. Two model objects were used in this work: one with delta functions at absorber edges approximating edge diffraction, and the other is a rectangular function representing geometric transmission (see Fig. 5(b)). Note that for numerical efficiency we have used only one edge in the models, which therefore correspond to a semi-infinite absorber screen. This is justified provided that the interaction between neighboring features is small, and also that the fields are symmetric about the center-line of the absorber. Given a coupling distance d, these models allow us to simultaneously estimate behavior for all values of absorber width using a single convolution. We now describe how the optimization was accomplished by way of the edge diffraction example of Fig 6(a).

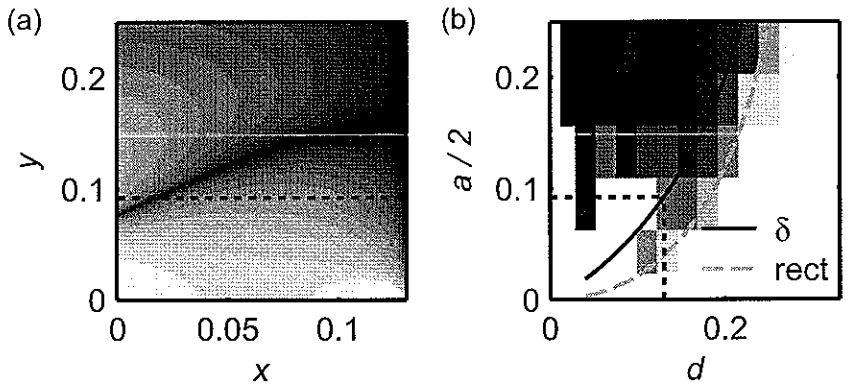

Fig. 6 Modeling of optimal absorber object tuning. (a) shows an example LSF for a case with $d = 0.125\lambda$, where the grayscale runs linearly from low (dark) to high (white). (b) shows a gray-scale map of real absorber image quality (dark being high contrast) as a function of absorber half-width $a/2$ and image thickness d, overlaid with the optimum curve for the edge-diffraction model (solid blue) and for geometric diffraction (dashed cyan curve).

One half of an LSF is shown in Fig 6(a), noting carefully that the object is at $x = d = 0.125\lambda$ and the mirror is at $x = 0$. If we use a single delta function for an edge object and ignore contributions from any neighboring edges, then Fig 6(a) also represents the blurring of the edge at $(x,y) = (0.125,0)$ into the region below the absorber ($y > 0$). Given an arbitrary absorber width a, then the line $y = a/2$ is the dark plane for that absorber, and the global dark intensity for (d,a) is the maximum intensity along the line. Minimizing global dark intensity against a yields optimum a for the given d, which in this case is represented by the dashed line in Fig. 6(a) and the point at the intersection of the dashed lines in Fig. 6(b). The blue curve in Fig. 6(b) shows optimum a as a function of d for this edge diffraction model, and the cyan curve shows the result for a geometric model using a similar process (the LSF was convolved with a step function).

The model curves are overlaid on a map of contrast from full simulations in Fig. 6(b), where black indicates high contrast regions in (d,a) space. This shows that the model predicts the minimum absorber width at a given depth-of-field, or alternatively the maximum depth-of-field for a given absorber width. The map also shows that the coupling distance is less critical for wider absorbers, and that there is a second optimum coupling for narrower absorbers. While these additional features are not conveyed by the model curves shown, the model does indeed predict them.

#84156 - $15.00 USD Received 14 Jun 2007; revised 20 Aug 2007; accepted 21 Aug 2007; published 27 Aug 2007

3.2 Interferometric imaging

Another interesting configuration is evanescent interferometric lithography [11], with only two plane waves incident with equal amplitude and opposite β, as shown in Fig. 7. In this case both electric field components should be considered ($I = |E_x|^2 + |E_y|^2$), and it can be shown that the image has planes of lateral symmetry that are null planes of either component. For integral order m the field is given by

$$e^{-i\alpha d}\omega\varepsilon E(x)/h^f = \begin{cases} \alpha\left(-e^{i\alpha x} + re^{i\alpha x}\right), \beta y = (2m+0)\pi/2 \\ \beta\left(-e^{i\alpha x} - re^{i\alpha x}\right), \beta y = (2m+1)\pi/2 \end{cases}. \quad (9)$$

where the upper solution corresponds to tangential-only planes (E_y) and the lower to normal-only planes (E_x).

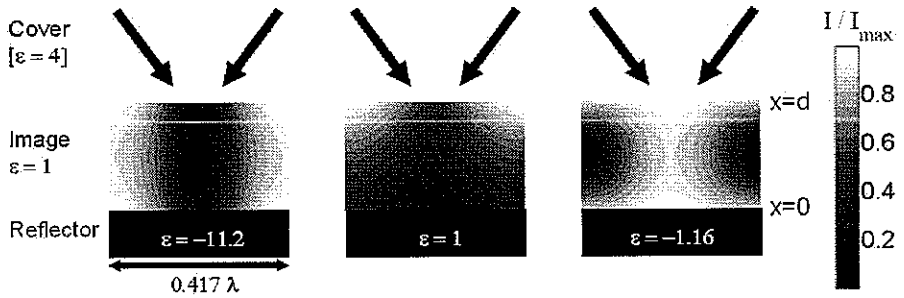

Fig. 7. Examples of evanescent interferometric images for different perfect reflectors ("+r" left and "-r"right) compared to the no reflection case (center). Note the rotation of the axes compared with the rest of the article. The incident waves shown result in near-evanescent condition $\beta/k = 1.2$, and equation (6) was used to choose permittivities for perfect symmetry.

Applying the reflection mapping for the negative case ($r = -e^{-i\alpha 2X}$) yields

$$E(x) \propto \begin{cases} |\alpha \cos[\alpha(x-X)]|, \beta y = (2m+0)\pi/2 \\ |\beta \sin[\alpha(x-X)]|, \beta y = (2m+1)\pi/2 \end{cases} \quad (10)$$

A null at X is predicted, allowing maximum local contrast which is not achieved without reflection. Uniformity and hence global contrast is maximised when $X = d/2$, requiring an appropriate reflectance that could be achieved using strategies such as described by Eq. (6). Maximum depth-of-field with reflection (corresponding to $\Gamma = 1$) is found by solving:

$$\begin{aligned} 1 &= |\cot[\alpha D/2]\alpha/\beta|, \beta < k \\ 1 &= |\csc[\alpha D/2]\alpha/\beta|, \beta > k \end{aligned} \quad (11)$$

The corresponding solution for the positive case is

$$\begin{aligned} 1 &= |\cot[\alpha D/2]\beta/\alpha|, \beta < k \\ 1 &= |\csc[\alpha D/2]\beta/\alpha|, \beta > k \end{aligned}, \quad (12)$$

and for the no-reflection case it is

$$1 = \exp[-\mathrm{Im}(\alpha)D]|\alpha/\beta|. \quad (13)$$

#84156 - $15.00 USD Received 14 Jun 2007; revised 20 Aug 2007; accepted 21 Aug 2007; published 27 Aug 2007

The different character of these three cases is compared in Fig. 7, where we have used Eq. (6) to choose optimum permittivities for an illustrative geometry ($\beta/k = 1.2$, $d = D$ for the right-most image). Here we see the different lateral positioning of the dark nulls due to the dominance of either the normal field (positive reflection, left) or the tangential field (negative reflection, right). In this particular case the positive reflection has the best global contrast, followed closely by negative reflection, both of which significantly outperform the non-reflecting case. We note that tuning the permittivity to the required value could be realized by appropriate choice of metal for the reflector and illumination wavelength.

Depth-of-field results for perfect reflectors are shown in Fig. 8, where D is dramatically improved in the evanescent regime ($\beta > k$). The positive case ($+r$) is slightly better because $|\beta| > |\alpha|$ when $\beta > k/2$, but as expected the negative case ($-r$) has less dispersion. As there is only one spatial frequency involved, perfect reflection is readily achievable, but low dispersion is probably still helpful.

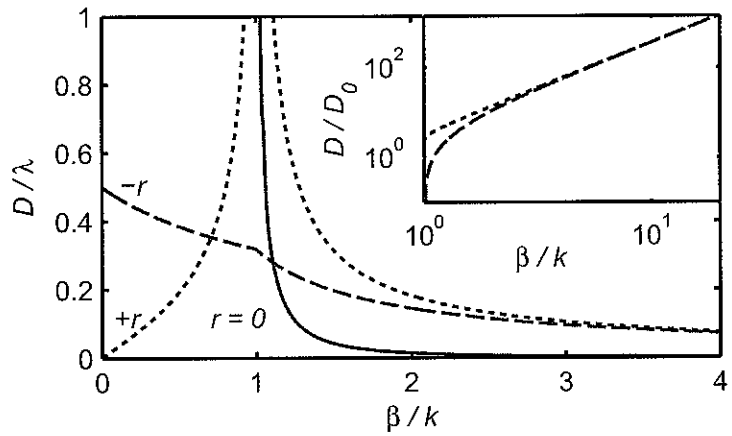

Fig. 8. Comparison of depth-of-field for interference imaging as a function of β: (main graph) absolute values and (inset) relative improvement of perfect positive ($+r$) and negative reflectors ($-r$) against no-reflection (r=0).

4. Conclusion

In conclusion, we have developed a general theory for evanescent field imaging with reflections using both spectral and spatial representations. We have shown why negative reflector permittivity improves uniformity and reduces blurring, explained the link between optimal coupling distance and absorber width for imaging of binary absorber objects, and explored improvements to evanescent interference lithography. Many of these examples will be of considerable practical use in evanescent imaging, and the theory can be readily applied to new geometries.

Acknowledgments

We gratefully acknowledge funding from the Marsden Fund of New Zealand (Contract UOC-312), and the University of Technology, Sydney. Helpful suggestions on this manuscript were provided by Martin Blaber and Michael Cortie.

#84156 - $15.00 USD Received 14 Jun 2007; revised 20 Aug 2007; accepted 21 Aug 2007; published 27 Aug 2007